

Glutamylation of the DNA sensor cGAS regulates its binding and synthase activity in antiviral immunity

Pengyan Xia^{1,6}, Buqing Ye^{1,6}, Shuo Wang^{1,6}, Xiaoxiao Zhu^{2,6}, Ying Du¹, Zhen Xiong^{1,3}, Yong Tian^{4,5} & Zuse Fan^{1,3}

Cyclic GMP-AMP synthase (cGAS) senses cytosolic DNA during viral infection and catalyzes synthesis of the dinucleotide cGAMP, which activates the adaptor STING to initiate antiviral responses. Here we found that deficiency in the carboxypeptidase CCP5 or CCP6 led to susceptibility to DNA viruses. CCP5 and CCP6 were required for activation of the transcription factor IRF3 and interferons. Polyglutamylation of cGAS by the enzyme TTLL6 impeded its DNA-binding ability, whereas TTLL4-mediated monoglutamylation of cGAS blocked its synthase activity. Conversely, CCP6 removed the polyglutamylation of cGAS, whereas CCP5 hydrolyzed the monoglutamylation of cGAS, which together led to the activation of cGAS. Therefore, glutamylation and deglutamylation of cGAS tightly modulate immune responses to infection with DNA viruses.

The innate immune system uses pattern-recognition receptors to detect microbial signatures (microbe-associated molecular patterns) or cellular damage (damage-associated molecular patterns)^{1,2}. Given that nucleic acids are central to the replication and propagation of pathogens, the recognition of aberrant RNA and DNA serves as a fundamental mechanism of host defense³. The activation of cytosolic nucleic acid receptors initiates the production of type I interferons and other cytokines and leads to the activation of adaptive immunity and restriction of infection^{4–6}.

Several DNA sensors, including Sox2 (ref. 7), TLR9 (ref. 8), AIM2 (ref. 9), DAI¹⁰, IFI16 (ref. 11) and DDX41 (ref. 12), have been reported to monitor pathogenic DNA that induces the secretion of type I interferons and proinflammatory cytokines. The cyclic GMP-AMP (cGAMP) synthase cGAS has been defined as a key sensor of cytosolic DNA^{13–15}. After binding DNA, cGAS catalyzes the synthesis of cGAMP, which in turn associates with and activates the adaptor STING and then elicits innate immune responses^{1,16,17}. However, it is still unknown how the activity of cGAS is regulated during host defense.

Post-translational modifications of proteins, such as phosphorylation, acetylation, ubiquitination and glycosylation, have important roles in regulating the activity of the target proteins during immune responses^{18,19}. Glutamylation adds glutamate side chains onto the γ -carboxyl groups of glutamic acid residues in the sequence of target proteins^{20,21}. Glutamylation is catalyzed by glutamylases, such as TTLL ('tubulin tyrosine ligase-like') enzymes^{22,23}. Glutamylation is a reversible modification akin to phosphorylation, whereby glutamates can be removed by a family of cytosolic carboxypeptidases (CCPs)²¹. Polyglutamylation of tubulins, the well-known targets of glutamylation, modulates the interaction between

microtubules and their partners, which regulates microtubule-related processes such as ciliary motility and neurite outgrowth^{21,24}. Glutamylation of the spindle-checkpoint protein Mad2 has a pivotal role in the development of megakaryocytes²⁵. Here we identified differential glutamylation of cGAS that regulated its activity in antiviral defense.

RESULTS

Susceptibility of CCP5- or CCP6-deficient mice to DNA viruses

Mice deficient in the gene encoding the cytosolic carboxypeptidase CCP6 (*Agbl4*; called 'Ccp6' here) display underdevelopment of megakaryocytes and abnormal thrombocytosis²⁵. We therefore sought to explore whether glutamylation was involved in the regulation of host defense against viral infection. In addition to mouse strains deficient in CCP1 (*Agtpbp1*; called 'Ccp1' here) and *Ccp6* studied before²⁵, we generated mouse strains deficient in the genes encoding CCP2 (*Agbl2*; called 'Ccp2' here), CCP3 (*Agbl3*; called 'Ccp3' here), CCP4 (*Agbl1*; called 'Ccp4' here) or CCP5 (*Agbl5*; called 'Ccp5' here) via genome-editing approached based on clustered regularly interspaced short palindromic repeats (CRISPR) and the endonuclease Cas9 (**Supplementary Fig. 1a**) and further verified deletion of these genes in bone marrow-derived macrophages (BMDMs) (**Fig. 1a**). We infected all six mutant mouse strains with DNA viruses such as herpes simplex virus (HSV) and vaccinia virus (VACV). We noted that mice deficient in *Ccp5* (*Ccp5*^{-/-}) or *Ccp6* (*Ccp6*^{-/-}) were more vulnerable to HSV and VACA infection than were the other mutant mice (**Fig. 1b** and **Supplementary Fig. 1b**). Moreover, *Ccp5*^{-/-} or *Ccp6*^{-/-} mice had lower concentrations of type I interferons in serum than did their wild type littermates, after infection with HSV (**Fig. 1c,d**). In contrast, mice deficient in *Ccp1*, *Ccp2*, *Ccp3* or *Ccp4* had concentrations of

¹Key Laboratory of Infection and Immunity of the Chinese Academy of Sciences, Institute of Biophysics, Chinese Academy of Sciences, Beijing, China. ²Animal Research Center, Institute of Biophysics, Chinese Academy of Sciences, Beijing, China. ³University of Chinese Academy of Sciences, Beijing, China. ⁴Key Laboratory of RNA Biology, Institute of Biophysics, Chinese Academy of Sciences, Beijing, China. ⁵Beijing Key Laboratory of Noncoding RNA, Institute of Biophysics, Chinese Academy of Sciences, Beijing, China. ⁶These authors contributed equally to this work. Correspondence should be addressed to Y.T. (ytian@ibp.ac.cn) or Z.F. (fanz@moon.ibp.ac.cn).

Received 7 September 2015; accepted 23 November 2015; published online 1 February 2016; corrected online 29 February 2016; doi:10.1038/ni.3356

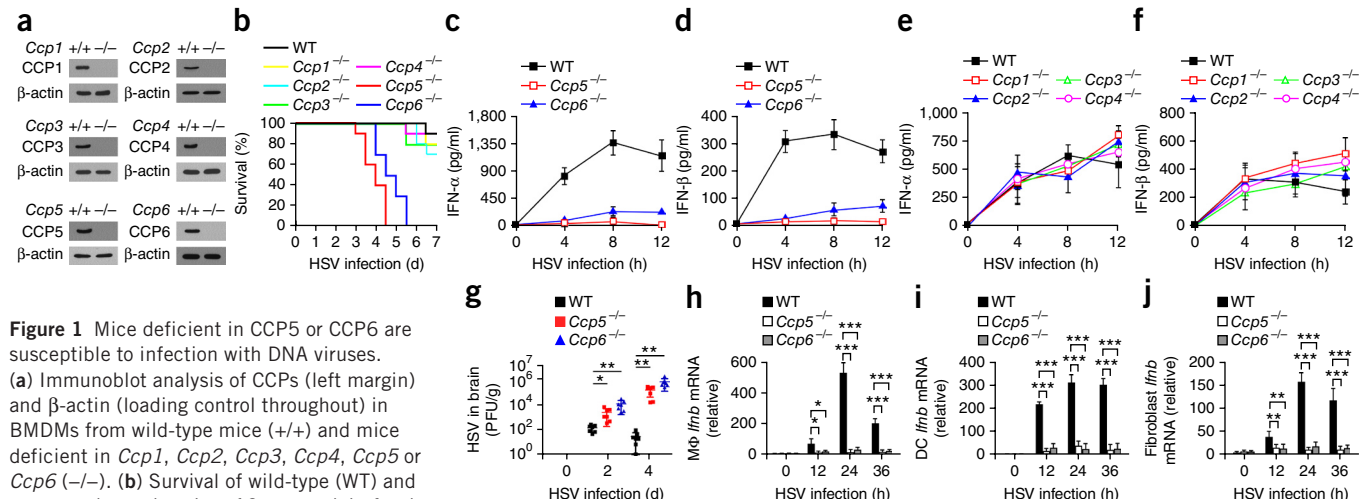


Figure 1 Mice deficient in CCP5 or CCP6 are susceptible to infection with DNA viruses. (a) Immunoblot analysis of CCPs (left margin) and β-actin (loading control throughout) in BMDMs from wild-type mice (+/+) and mice deficient in *Ccp1*, *Ccp2*, *Ccp3*, *Ccp4*, *Ccp5* or *Ccp6* (−/−). (b) Survival of wild-type (WT) and mutant mice as in a ($n = 10$ per strain) after intravenous injection of HSV (1×10^6 plaque-forming units (PFU) per mouse). (c,d) Enzyme-linked immunosorbent assay (ELISA) of IFN-α (c) and IFN-β (d) in serum obtained from wild-type, *Ccp5*−/− and *Ccp6*−/− mice ($n = 9$ per strain) at various times (horizontal axes) after intravenous injection of HSV (1×10^7 PFU per mouse). (e,f) ELISA of IFN-α (e) and IFN-β (f) in serum obtained from wild-type, *Ccp1*−/−, *Ccp2*−/−, *Ccp3*−/− and *Ccp4*−/− mice ($n = 7$ per strain) after intravenous injection of HSV (1×10^7 PFU per mouse). (g) Viral titers in homogenates of brains from wild-type, *Ccp5*−/− and *Ccp6*−/− mice ($n = 7$ per strain) after intravenous injection of HSV (1×10^6 PFU per mouse). (h–j) RT-PCR analysis of *Ifnb* mRNA in peritoneal macrophages (MΦ) (h), peripheral CD11ch1 DCs (i) and lung fibroblasts (j) obtained from wild-type, *Ccp5*−/− and *Ccp6*−/− mice ($n = 5$ per cell type) after intravenous injection of HSV (1×10^7 PFU per mouse); results are presented relative to those of wild-type cells immediately after infection with HSV (0 h). * $P < 0.05$, ** $P < 0.01$ and *** $P < 0.001$ (Student's *t*-test). Data are representative of at least three independent experiments (mean and s.d. in c–j).

type I interferons in serum similar to those of their wild-type littermates after infection with HSV (Fig. 1e,f). Consistent with that, after infection with HSV, viral titers were much higher in *Ccp5*- or *Ccp6*-deficient mouse brains than in their wild-type counterparts (Fig. 1g). At the same time, after infection with HSV, viral titers in mice deficient in *Ccp1*, *Ccp2*, *Ccp3* or *Ccp4* were similar to those of their wild-type counterparts (Supplementary Fig. 1c). Similar results were obtained by infection with VACV (Supplementary Fig. 1d–f).

We then assessed interferon-encoding mRNA in *Ccp5*- or *Ccp6*-deficient cells of the innate immune system following viral infection. As expected, after infection with HSV, *Ccp5*- or *Ccp6*-deficient cells had much lower expression of *Ifnb* mRNA (encoding interferon-β (IFN-β)) than did their wild-type counterparts after infection with HSV (Fig. 1h–j). In contrast, cells of the innate immune system from mice deficient in *Ccp1*, *Ccp2*, *Ccp3* or *Ccp4* had expression of *Ifnb* mRNA similar to that of their wild-type counterparts after infection with HSV (Supplementary Fig. 1g–i). Similar observations were obtained with VACV-infected *Ccp5*- or *Ccp6*-deficient cells (data not shown). These results indicated involvement of CCP5 and CCP6 in regulating immune responses to DNA viruses.

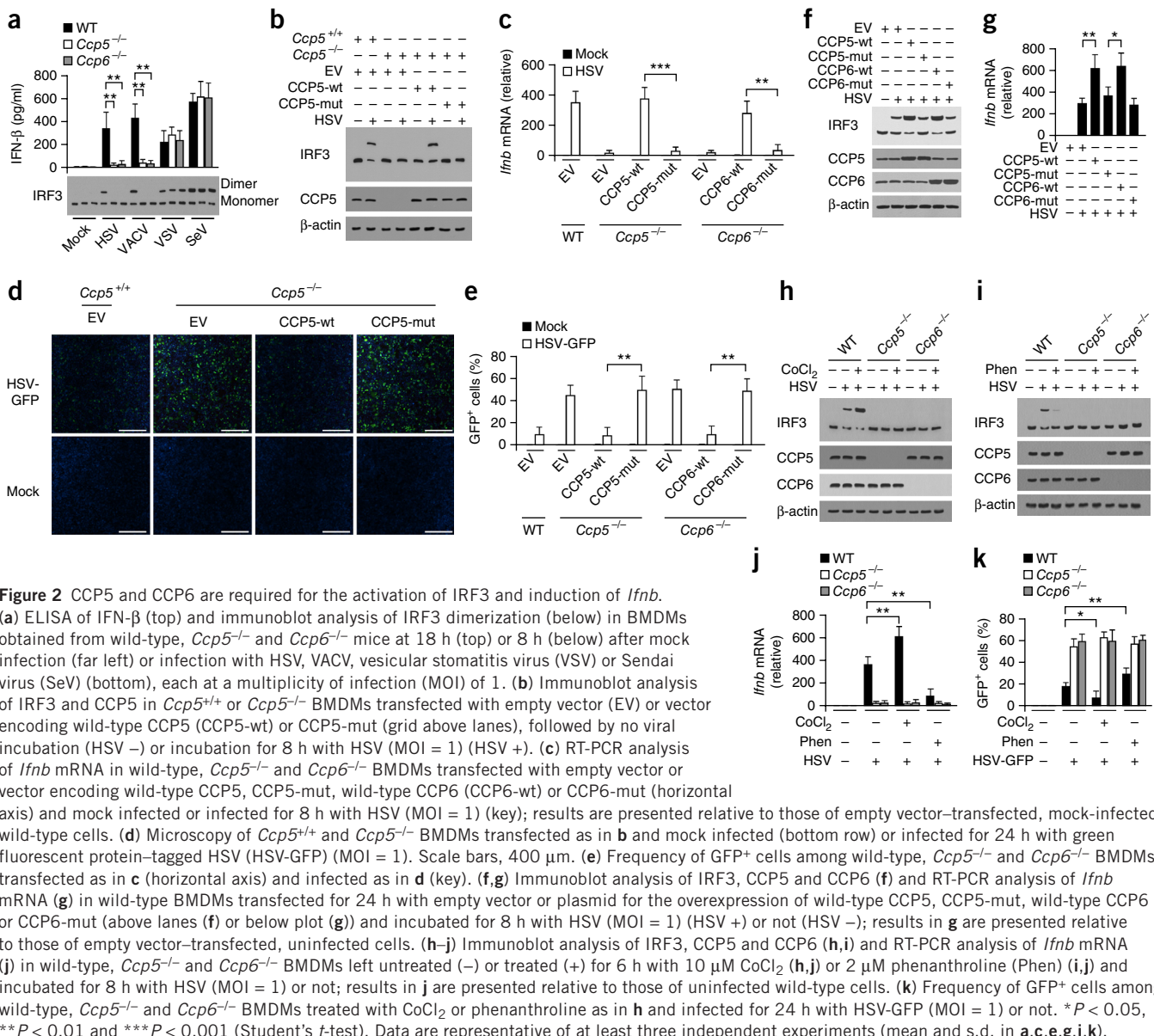
Requirement for CCP5 and CCP6 in *Ifnb* induction

We next sought to assess the innate immune responses of BMDMs to viral challenge by analyzing the activation of the transcription factor IRF3, which undergoes homodimerization after it is phosphorylated²⁶. We observed that *Ccp5*- or *Ccp6*-deficient BMDMs failed to trigger activation (homodimerization) of IRF3 or production of IFN-β following infection with a DNA virus (Fig. 2a). However, after challenge with an RNA virus, *Ccp5*- or *Ccp6*-deficient BMDMs were able to induce IRF3 activation and IFN-β secretion (Fig. 2a). Consistent with that, transfection of herring testis DNA or *Escherichia coli* DNA did not induce activation of IRF3 or secretion of IFN-β from *Ccp5*- or *Ccp6*-deficient BMDMs (Supplementary Fig. 2a). As expected, the synthetic RNA duplex poly(I:C) triggered IRF3

activation and IFN-β production in *Ccp5*−/− or *Ccp6*−/− BMDMs (Supplementary Fig. 2a). These data confirmed the proposal that CCP5 and CCP6 were specifically involved in the regulation of immune responses to DNA viruses but not those to RNA viruses.

To determine whether the enzymatic activity of CCP5 and CCP6 was required for the activation of IRF3, we generated enzymatically inactive mutants of CCP5 (CCP5-mut; with the substitutions H252S and E255Q)²¹ and CCP6 (CCP6-mut; with the substitutions H230S and E233Q)²⁵. We then restored expression of CCP5 in *Ccp5*−/− BMDMs via wild-type CCP5 or CCP5-mut. We found that restoration with CCP5-mut resulted in no activation of IRF3 after infection with HSV, whereas wild-type CCP5 triggered IRF3 activation (Fig. 2b). In parallel, restoration of the expression of CCP6 in *Ccp6*−/− BMDMs via CCP6-mut resulted in no activation of IRF3 after infection with HSV (Supplementary Fig. 2b). Consequently, similar restoration via CCP5-mut or CCP6-mut did not induce *Ifnb* expression after challenge with HSV, whereas similar restoration with wild-type CCP5 or wild-type CCP6 did initiate elevated expression of *Ifnb* after challenge with HSV (Fig. 2c). Restoration via CCP5-mut and CCP6-mut did not eradicate HSV infection (Fig. 2d,e and Supplementary Fig. 2c). To further define the direct effect of CCP5 and CCP6 on IRF3 activation and interferon production, we overexpressed CCP5 or CCP6 in wild-type BMDMs. As expected, overexpression of CCP5 or CCP6 augmented IRF3 activation and IFN-β expression after challenge with HSV (Fig. 2f,g), and promoted restriction of HSV propagation (Supplementary Fig. 2d). These results indicated that the deglutamyl hydrolysis activity of CCP5 and CCP6 was required for the induction of IRF3 activation and IFN-β production during infection with a DNA virus.

CoCl_2 is an agonist for carboxypeptidases²⁷, and phenanthroline serves as an inhibitor of carboxypeptidases²¹. We noted that after infection with HSV, treatment with CoCl_2 substantially enhanced IRF3 activation in wild-type BMDMs, whereas such IRF3 activation was abrogated in *Ccp5*−/− or *Ccp6*−/− cells infected with HSV



and treated with CoCl₂ (Fig. 2h). Conversely, treatment with phenanthroline hindered the activation of IRF3 in wild-type BMDMs (Fig. 2i). Consequently, after challenge with HSV, treatment with CoCl₂ increased *Ifnb* expression and antiviral activity in wild-type BMDMs but not in *Ccp5*^{-/-} or *Ccp6*^{-/-} BMDMs (Fig. 2j,k and Supplementary Fig. 2e,f). In contrast, treatment with phenanthroline decreased *Ifnb* expression and antiviral activity in wild-type BMDMs but not in *Ccp5*^{-/-} or *Ccp6*^{-/-} BMDMs (Fig. 2j,k and Supplementary Fig. 2e,f). In addition, treatment with CoCl₂ or phenanthroline did not affect *Ifnb* expression after infection of wild-type BMDMs or even *Ccp5*^{-/-} or *Ccp6*^{-/-} BMDMs with vesicular stomatitis virus (Supplementary Fig. 2g). This confirmed the proposal that CCP5- or CCP6-mediated deglutamylation participated in the regulation of antiviral responses to DNA viruses.

cGAS as a substrate for CCP5 and CCP6

We next sought to identify candidate substrates for deglutamylation during antiviral responses to DNA viruses. The antibody GT335

specifically recognizes the branch points of glutamate side chains and detects all glutamylated forms of target proteins²¹. After immunoblot analysis, two bands of around 58 kilodaltons (kDa) and 50 kDa appeared in the lanes for lysates of BMDMs and dendritic cells (DCs) from CCP5-deficient mice (Fig. 3a). The upper band (58 kDa) was undetectable and the lower band (50 kDa) had diminished intensity in the corresponding lanes for lysates of BMDMs and DCs from their wild-type littermates (Fig. 3a). Thus, these two bands might have represented proteins that could be potential substrates for CCP5. We next generated wild-type CCP5 and CCP5-mut and immobilized them on affinity resin for neutral or basic proteins, for passage through BMDM lysates by affinity chromatography. The eluted fractions were resolved by SDS-PAGE, followed by silver staining (Fig. 3b). These two bands were present in the gel analyzing CCP5-mut and were cut for mass spectrometry. The lower, 50-kDa band was identified as α -tubulin (data not shown), a reported CCP5 substrate²¹. The upper, 58-kDa band was identified as cGAS (Supplementary Fig. 3a), a previously unknown candidate substrate for CCP5.

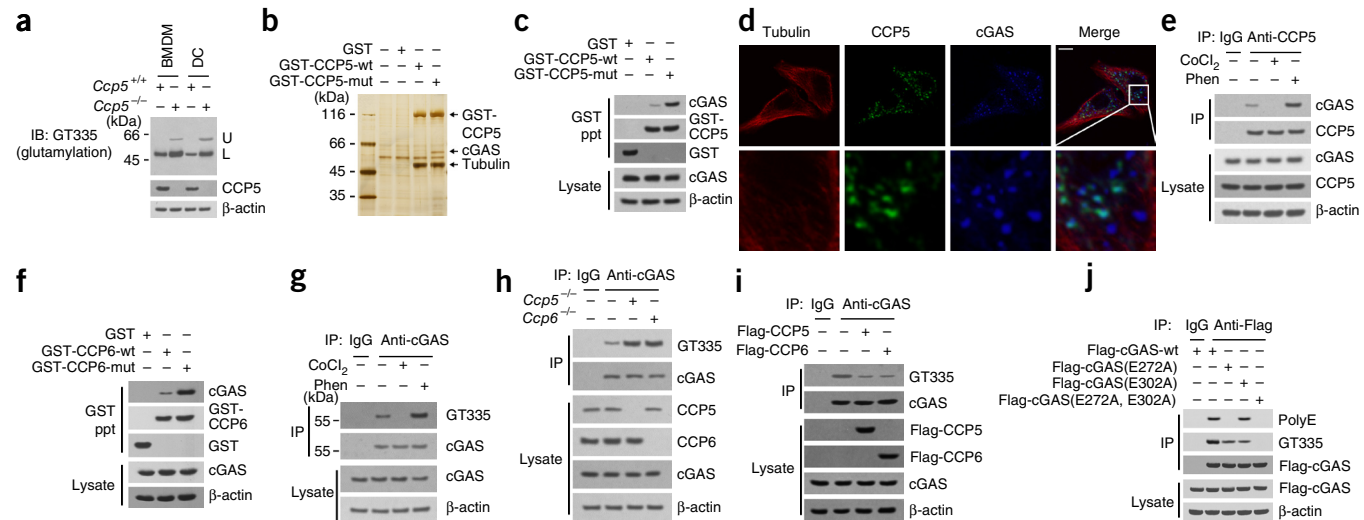


Figure 3 cGAS is a substrate for CCP5 and CCP6. (a) Immunoblot analysis of glutamylated (assessed with GT335; top) and of CCP5 (below) in *Ccp5*^{+/+} and *Ccp5*^{-/-} BMDMs and DCs. (b) Affinity chromatography of glutathione S-transferase (GST) alone or GST-tagged wild-type CCP5 or CCP5-mut immobilized on affinity resins, assessed by the addition of BMDM lysates, resolution of the eluted fractions by SDS-PAGE and silver staining (presented here), followed by liquid chromatography-linear trap quadrupole tandem mass spectrometry of the 58-kDa and 50-kDa bands (Supplementary Fig. 3a). Left margin, size in kDa. (c) GST-precipitation assay of GST or GST-tagged wild-type CCP5 or CCP5-mut incubated for 4 h with BMDM lysates, assessed by immunoblot analysis of cGAS, GST-tagged CCP5 or GST among the precipitates (GST ppt) and of cGAS in lysates without precipitation (below). (d) Confocal microscopy of wild-type BMDMs stained with antibody to (anti-) β-tubulin, anti-cGAS and anti-CCP5. Area outlined at top right is enlarged 6x in row below. Scale bar, 10 μm. (e) Immunoassay of wild-type BMDMs left untreated (−) or treated (+) for 6 h with 10 μM CoCl₂ or 2 μM phenanthroline (above lanes), assessed by immunoprecipitation (IP) with immunoglobulin G (IgG), as a control, or with anti-CCP5 and immunoblot analysis of immunoprecipitates (top two blots) and total lysates (below) with anti-cGAS or anti-CCP5. (f) GST-precipitation assay of GST or GST-tagged wild-type CCP6 or CCP6-mut incubated for 4 h with BMDM lysates, assessed by immunoblot analysis of cGAS, GST-tagged CCP6 or GST among the precipitates (GST ppt) and of cGAS in lysates without precipitation (below). (g) Immunoassay of wild-type BMDMs treated as in e, assessed by immunoprecipitation with IgG or anti-cGAS and immunoblot analysis of immunoprecipitates with GT335 or anti-cGAS and of total lysates with anti-cGAS. (h) Immunoassay of *Ccp5*^{-/-} and *Ccp6*^{-/-} BMDMs by immunoprecipitation with IgG or anti-cGAS and immunoblot analysis of immunoprecipitates with GT335 or anti-cGAS and of total lysates with anti-CCP5, anti-CCP6 or anti-cGAS. (i) Immunoassay of wild-type BMDMs left untransfected (−) or transfected (+) for 24 h with vector encoding Flag-tagged CCP5 or CCP6, assessed by immunoprecipitation with IgG or anti-cGAS and immunoblot analysis of immunoprecipitates with GT335 or anti-cGAS and of total lysates with anti-Flag or anti-cGAS. (j) Immunoassay of wild-type BMDMs left untransfected (−) or transfected (+) for 24 h with vector encoding Flag-tagged wild-type cGAS (cGAS-wt), cGAS(E272A), cGAS(E302A) or cGAS(E272A,E302A), assessed by immunoprecipitation with IgG or anti-Flag and immunoblot analysis with polyE, GT335 or anti-Flag and of total lysates with anti-Flag. Data are representative of at least three independent experiments.

CCP5-mut was able to precipitate cGAS from BMDM lysates (Fig. 3c). Colocalization of cGAS with CCP5 in the cytoplasm of BMDMs was visualized by confocal microscopy (Fig. 3d). Moreover, the colocalization of cGAS with CCP5 did not overlap with microtubular structures (Fig. 3d). Staining of cGAS displayed punctate structures (Fig. 3d), as previously observed¹⁵. Moreover, the CCP inhibitor phenanthroline augmented the association between CCP5 and cGAS, whereas treatment with CoCl₂ abrogated this association (Fig. 3e). Notably, deletion of CCP5's enzymatic domain (residues 160–424) abolished the interaction between CCP5 and cGAS (Supplementary Fig. 3b), which suggested that the interaction of CCP5 with cGAS required the enzymatic activity of CCP5. As noted for CCP5, the interaction of CCP6 with cGAS was also verified (Fig. 3f and Supplementary Fig. 3c,d). The interaction of CCP6 with cGAS was also dependent on its enzymatic activity (Supplementary Fig. 3e). Collectively, these results indicated that the association of cGAS with CCP5 or CCP6 required the enzymatic activity of CCP5 or CCP6, which suggested that cGAS might be a potential substrate for CCP5 and CCP6.

Notably, recombinant CCP5-mut or CCP6-mut did not precipitate together with recombinant cGAS (data not shown), whereas CCP5-mut or CCP6-mut bound to endogenous cGAS (Fig. 3c,f). These results suggested that CCP5 or CCP6 might need to bind to glutamylated cGAS for their hydrolysis. Indeed, cGAS was glutamylated in BMDMs (Fig. 3g). Moreover, treatment with the CCP inhibitor

phenanthroline substantially enhanced the glutamylation of cGAS, whereas the CCP agonist CoCl₂ rendered the glutamylation of cGAS undetectable (Fig. 3g). More notably, more glutamylation of cGAS was observed in *Ccp5*^{-/-} and *Ccp6*^{-/-} BMDMs than in wild-type cells (Fig. 3h). In contrast, overexpression of CCP5 or CCP6 decreased the glutamylation of cGAS (Fig. 3i). Additionally, CCP1, CCP2, CCP3 and CCP4 failed to precipitate together with cGAS in BMDM lysates (data not shown). Finally, deficiency in *Ccp1*, *Ccp2*, *Ccp3* or *Ccp4* did not affect the glutamylation of cGAS (data not shown). Therefore, in these conditions, cGAS was a substrate for both CCP5 and CCP6 but not for other CCPs.

Deglutamylation of cGAS by CCP5 and CCP6

Glutamylation is the ATP-dependent addition of glutamates catalyzed by glutamylases of the TTLL family, either singly or sequentially²⁰. As noted above, the antibody GT335 can recognize branch-point glutamates, while the polyglutamylated-specific antibody polyE is able to detect three or more consecutive branched glutamates²¹. On the basis of amino acid mapping and structural prediction of cGAS, we identified two putative glutamylated sites on mouse cGAS (Supplementary Fig. 3f–h). We then substituted alanine for the glutamic acid at positions 272 (E272A) and 302 (E302A), separately or together, and transfected vector encoding these mutants into BMDMs. We found that cGAS(E272A) had branched glutamates that

were detected only by GT335, whereas cGAS(E302A) had branched glutamates that were detected by both GT335 and polyE (Fig. 3j). Moreover, the double mutant cGAS(E272A,E302A) lacked branched glutamates (Fig. 3j). These results suggested that cGAS had three or more glutamates added at Glu272 and two or fewer glutamates at Glu302.

We next investigated how cGAS was deglutamylated by CCP5 and CCP6. We cotransfected BMDMs with vector encoding cGAS(E272A) or cGAS(E302A), together with vector encoding CCP5 or CCP6, and assessed the cells by immunoblot analysis. We observed that overexpression of CCP5 abolished the GT335 signals for BMDMs transfected to express cGAS(E272A) but not in those transfected to express cGAS(E302A) (Supplementary Fig. 4a). In contrast, overexpression of CCP6 eliminated the GT335 signals for BMDMs transfected to express cGAS(E302A) but not those transfected to express cGAS(E272A) (Supplementary Fig. 4b). Moreover, *Ccp5*-deficient BMDMs overexpressing cGAS(E272A) displayed stronger GT335 signals than those in similarly transfected wild-type

cells, whereas overexpression of cGAS(E302A) had no such effect (Supplementary Fig. 4c). In addition, overexpression of cGAS(E302A) in *Ccp6*-deficient cells resulted in stronger GT335 and polyE signals than those of similarly transfected wild-type cells, while overexpression of cGAS(E272A) did not influence GT335 signals of immunoprecipitated cGAS (Supplementary Fig. 4d). As expected, CCP5-mut associated with cGAS(E272A) but not with cGAS(E302A) in lysates of wild-type BMDMs transfected to express these (Supplementary Fig. 4e). In contrast, CCP6-mut interacted with cGAS(E302A) but not with cGAS(E272A) in lysates of wild-type BMDMs transfected to express these (Supplementary Fig. 4f). Therefore, CCP5 was responsible for hydrolyzing the glutamate chain of cGAS at E302, and CCP6 removed the glutamate chain of cGAS at Glu272.

Differential glutamylation of cGAS by TTLL4 and TTLL6

To further determine how the glutamylases catalyzed the glutamylation of cGAS, we screened nine glutamylases for their interactions with cGAS. We found that only TTLL4 and TTLL6 associated with

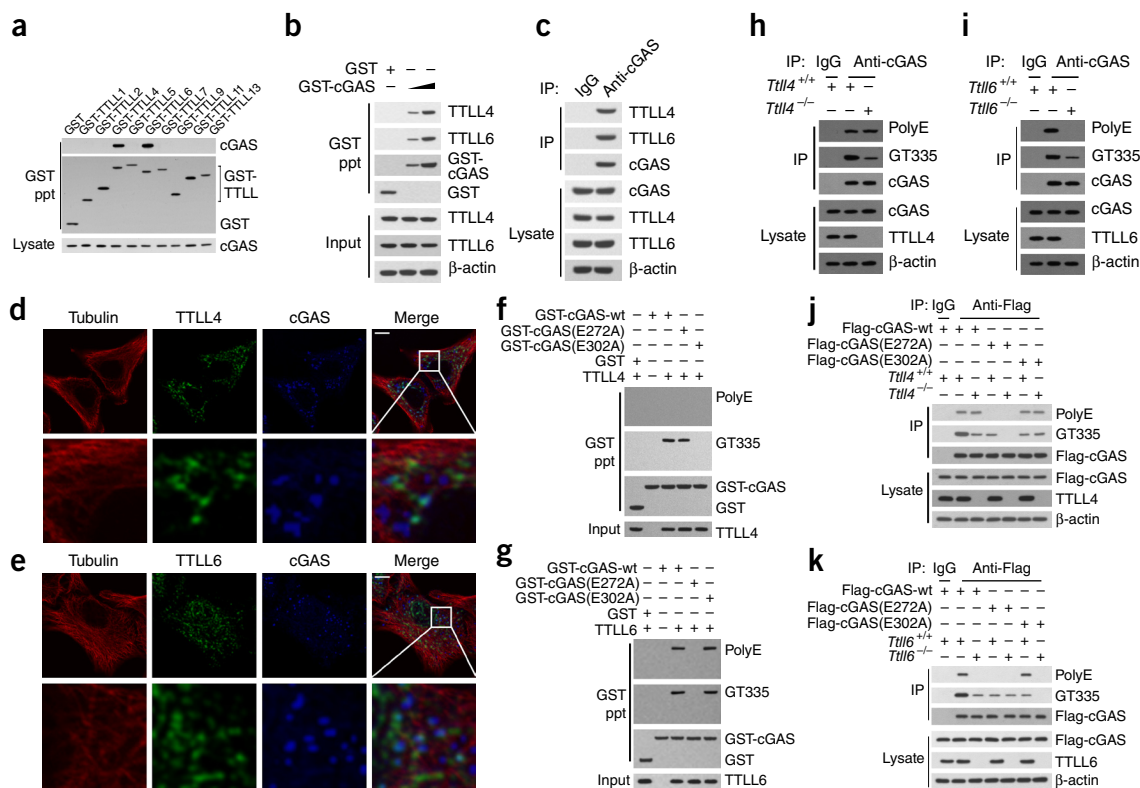
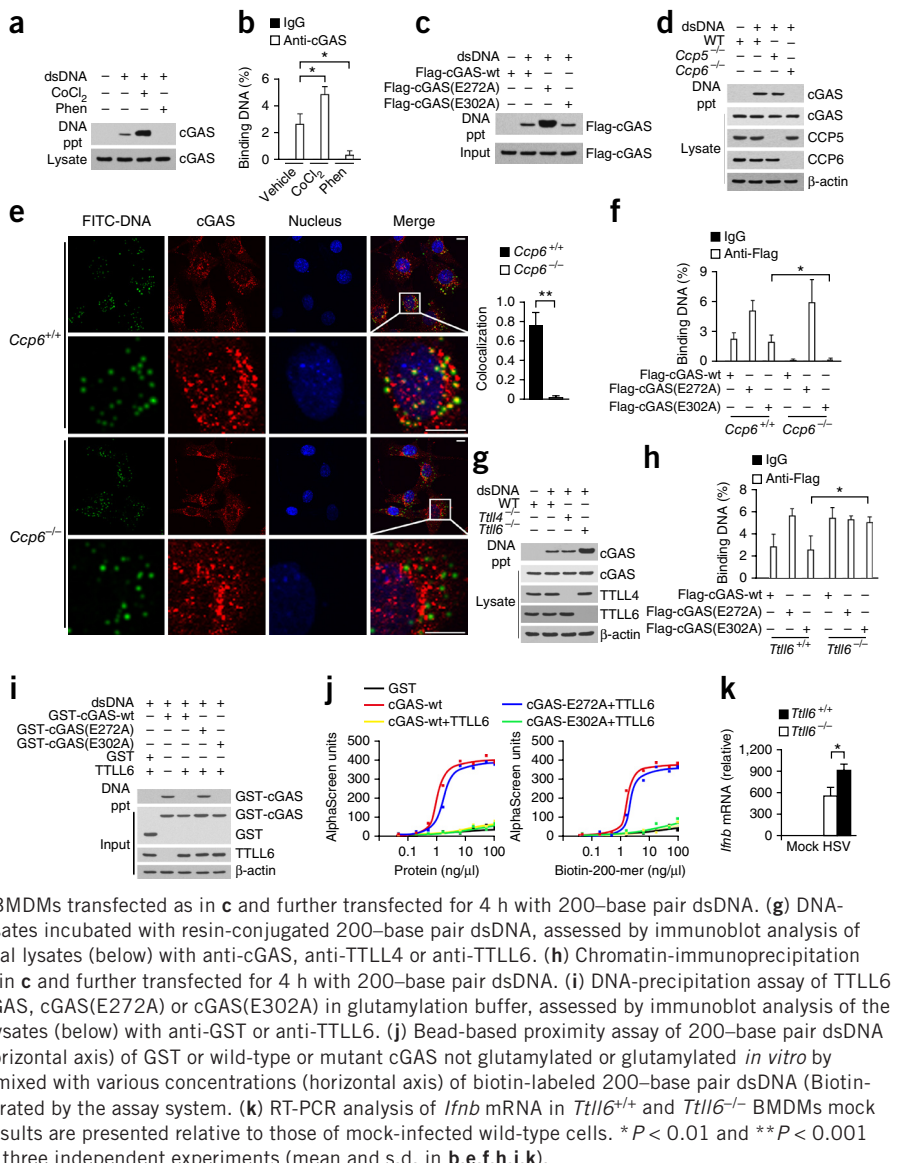


Figure 4 cGAS is glutamylated differentially by TTLL4 and TTLL6. (a) GST-precipitation assay of GST or GST-tagged members of the TTLL family (above lanes) incubated for 4 h with BMDM lysates, assessed by immunoblot analysis of cGAS, GST-tagged TTLL glutamylases or GST among the precipitates (GST ppt) and of cGAS in lysates without precipitation (below). (b) GST-precipitation assay of GST or increasing amounts (wedge) of GST-cGAS incubated for 4 h with BMDM lysates, assessed by immunoblot analysis of TTLL4, TTLL6, GST-tagged cGAS or GST among the precipitates (GST ppt) and of TTLL4 and TTLL6 in lysates without precipitation (below). (c) Immunoblot of wild-type BMDMs subjected to immunoprecipitation with IgG or anti-cGAS, assessed by immunoblot analysis of immunoprecipitates (top three blots) or total lysates (below) with anti-TTLL4, anti-TTLL6 or anti-cGAS. (d,e) Confocal microscopy of wild-type BMDMs stained with anti-β-tubulin, anti-cGAS and anti-TTLL4 (d) or anti-TTLL6 (e). Area outlined at top right is enlarged 5x in row below. Scale bars, 10 μm. (f,g) GST-precipitation assay of Flag-tagged TTLL4 (f) or TTLL6 (g) overexpressed for 24 h in mouse embryonic fibroblasts (+) or not (-), followed by immunoprecipitation with anti-Flag and elution with Flag peptides, then incubation of immunoprecipitates for 1 h with GST or GST-tagged wild-type cGAS, cGAS(E272A) or cGAS(E302A) in glutamylating buffer, assessed by immunoblot analysis of the precipitates with polyE, GT335 or anti-GST (GST ppt) and of total lysates (below) with anti-TTLL4 (f) or anti-TTLL6 (g). (h,i) Immunoblot of *Ttll4*^{+/+} and *Ttll4*^{-/-} BMDMs (h) or *Ttll6*^{+/+} and *Ttll6*^{-/-} BMDMs (i) by immunoprecipitation with IgG or anti-cGAS and immunoblot analysis of the immunoprecipitates with polyE, GT335 or anti-cGAS (top three blots) and of total lysates (below) with anti-cGAS and anti-TTLL4 (h) or anti-TTLL6 (i). (j,k) Immunoblot of *Ttll4*^{+/+} and *Ttll4*^{-/-} BMDMs (j) or *Ttll6*^{+/+} and *Ttll6*^{-/-} BMDMs (k) left untransfected (-) or transfected (+) for 24 h to express Flag-tagged wild-type cGAS, cGAS(E272A) or cGAS(E302A), assessed by immunoprecipitation with IgG or anti-Flag and immunoblot analysis of the immunoprecipitates with polyE, GT335 or anti-Flag (top three blots) and of total lysates (below) with anti-Flag and anti-TTLL4 (j) or anti-TTLL6 (k). Data are representative of at least three independent experiments.

Figure 5 TTLL6-mediated polyglutamylation of cGAS suppresses its DNA-binding ability. (a) DNA-precipitation assay of untreated lysates alone (far left) or BMDM lysates pretreated (+) or not (−) with 10 μ M CoCl₂ or 2 μ M phenanthroline (above lanes) and incubated with resin-conjugated 200-base pair dsDNA, assessed by immunoblot analysis of the precipitates (DNA ppt) and total lysates (below) with anti-cGAS. (b) Chromatin-immunoprecipitation assay (with anti-cGAS) of BMDMs treated with vehicle, CoCl₂ or phenanthroline (horizontal axis) and transfected with 200-base pair dsDNA. (c) DNA-precipitation assay of lysates of BMDMs transfected to express Flag-tagged wild-type cGAS, cGAS(E272A) or cGAS(E302A) and incubated with resin-conjugated 200-base pair dsDNA (+) or not (−), assessed by immunoblot analysis of the precipitates (DNA ppt) and total lysates (below) with anti-Flag. (d) DNA-precipitation assay of *Ccp5*^{−/−} and *Ccp6*^{−/−} BMDM lysates incubated with resin-conjugated 200-base pair dsDNA (+) or not (−), assessed by immunoblot analysis of the precipitates (DNA ppt) with anti-cGAS and of total lysates (below) with anti-cGAS, anti-CCP5 or anti-CCP6. (e) Confocal microscopy of *Ccp6*^{+/+} and *Ccp6*^{−/−} BMDMs transfected with fluorescein isothiocyanate (FITC)-conjugated 50-base pair dsDNA (left), and colocalization of cGAS with the labeled DNA at left (Pearson's correlation coefficient; right). Area outlined (top right image of each pair at left) is enlarged 5x in row below. Scale bars (left), 10 μ m. (f) Chromatin-immunoprecipitation assay of *Ccp6*^{+/+} and *Ccp6*^{−/−} BMDMs transfected as in c and further transfected for 4 h with 200-base pair dsDNA. (g) DNA-precipitation assay of *Ttll4*^{−/−} and *Ttll6*^{−/−} BMDM lysates incubated with resin-conjugated 200-base pair dsDNA, assessed by immunoblot analysis of the precipitates (DNA ppt) with anti-cGAS and of total lysates (below) with anti-cGAS, anti-TTLL4 or anti-TTLL6. (h) Chromatin-immunoprecipitation assay of *Ttll6*^{+/+} and *Ttll6*^{−/−} BMDMs transfected as in c and further transfected for 4 h with 200-base pair dsDNA. (i) DNA-precipitation assay of TTLL6 incubated for 1 h with GST, GST-tagged wild-type cGAS, cGAS(E272A) or cGAS(E302A) in glutamylating buffer, assessed by immunoblot analysis of the precipitates (DNA ppt) with anti-GST or anti-TTLL6. (j) Bead-based proximity assay of 200-base pair dsDNA (50 ng/ μ l) incubated with various concentrations (horizontal axis) of GST or wild-type or mutant cGAS not glutamylated or glutamylated *in vitro* by TTLL6 (+TTLL6) (left) or cGAS as at left (50 ng/ μ l) mixed with various concentrations (horizontal axis) of biotin-labeled 200-base pair dsDNA (Biotin-200-mer) (right); results are presented in units generated by the assay system. (k) RT-PCR analysis of *Ifnb* mRNA in *Ttll4*^{+/+} and *Ttll6*^{−/−} BMDMs mock infected or incubated for 8 h with HSV (MOI = 1); results are presented relative to those of mock-infected wild-type cells. * P < 0.01 and ** P < 0.001 (Student's *t*-test). Data are representative of at least three independent experiments (mean and s.d. in b,e,f,h,j,k).

cGAS (Fig. 4a). Furthermore, TTLL4 and TTLL6 showed high constitutive expression in cells of the mouse innate immune system, such as BMDMs, DCs and fibroblasts (Supplementary Fig. 4g). The interaction of cGAS with TTLL4 and TTLL6 was verified by a precipitation assay (Fig. 4b,c). cGAS localized together with TTLL4 and TTLL6 in the cytoplasm of BMDMs, and this colocalization did not overlap with microtubular structures (Fig. 4d,e). These observations suggested that TTLL4- and TTLL6-mediated modifications of cGAS were not restricted to microtubular structures. It has been reported that TTLL4 is a monoglutamylase and that TTLL6 polyglutamylates tubulins²³. After incubation with TTLL4 in an *in vitro* glutamylating system, GT335 (glutamate) signals appeared (by immunoblot analysis) only for samples containing wild-type cGAS or cGAS(E272A), not those containing cGAS(E302A) (Fig. 4f), which suggested that cGAS was monoglutamylated by TTLL4 at Glu272. In contrast, following incubation with TTLL6, both GT335 and polyE signals were present (by immunoblot analysis) for samples containing wild-type cGAS or cGAS(E302A) but not those



containing cGAS(E272A) (Fig. 4g), which indicated that cGAS was polyglutamylated by TTLL6 at Glu272.

Through domain mapping, we found that TTLL4 interacted with a fragment consisting of residues 280–320 of cGAS, whereas TTLL6 associated with a fragment consisting of residues 240–280 of cGAS (Supplementary Fig. 4h). Additionally, TTLL4 and TTLL6 associated with wild-type cGAS or either cGAS mutant (Supplementary Fig. 4i,j), which suggested that the interaction of cGAS with TTLL4 and TTLL6 was independent of the glutamylation of cGAS. We next generated *Ttll4*- or *Ttll6*-deficient mice via CRISPR-Cas9 technology (Supplementary Fig. 4k). We noted that the GT335 signals for immunoprecipitated cGAS were substantially diminished in *Ttll4*^{−/−} BMDMs, whereas polyE signals were unchanged, relative to those in wild-type cells, as detected by immunoblot analysis (Fig. 4h). In contrast, polyE signals for immunoprecipitated cGAS were undetectable and GT335 signals were substantially diminished in *Ttll6*^{−/−} BMDMs, relative to those in wild-type cells, as detected by immunoblot analysis (Fig. 4i). Finally, restoration of *Ttll4*^{−/−} BMDMs with cGAS(E272A)

did not result in GT335 signals, whereas *Ttll4*^{-/-} BMDMs restored with cGAS(E302A) displayed GT335 signals, as detected by immunoblot analysis (Fig. 4j). In parallel, restoration of *Ttll6*^{-/-} BMDMs with cGAS(E272A) resulted in GT335 signals of cGAS but a lack of polyE signals, whereas restoration of *Ttll6*^{-/-} BMDMs with cGAS(E302A) impaired both GT335 signals and polyE signals of cGAS, as detected by immunoblot analysis (Fig. 4k). cGAS was therefore glutamylated differentially by TTLL4 and TTLL6.

cGAS polyglutamylation suppresses its DNA-binding ability

After binding DNA, cGAS undergoes a conformational change to catalyze cGAMP synthesis^{28,29}. To investigate whether glutamylation of cGAS affected its DNA-binding ability, we performed a DNA-precipitation

assay using cell lysates pretreated with the CCP agonist CoCl₂ or the inhibitor phenanthroline. After treatment with CoCl₂, more cGAS associated with double-stranded DNA (dsDNA) (Fig. 5a). In contrast, after treatment with phenanthroline, less cGAS was precipitated by dsDNA (Fig. 5a). To further analyze the DNA-binding ability of cGAS *in vivo*, we transfected dsDNA into BMDMs, followed by incubation of the cells with CoCl₂ or phenanthroline. Consistent with the results reported above, in the presence of phenanthroline, cGAS associated with less dsDNA in BMDMs, whereas it bound much more dsDNA in the presence of CoCl₂ (Fig. 5b). These results suggested that glutamylation of cGAS impeded its DNA-binding ability.

We next sought to determine which glutamic acid's glutamylation affected the DNA-binding ability of cGAS. We transfected dsDNA,

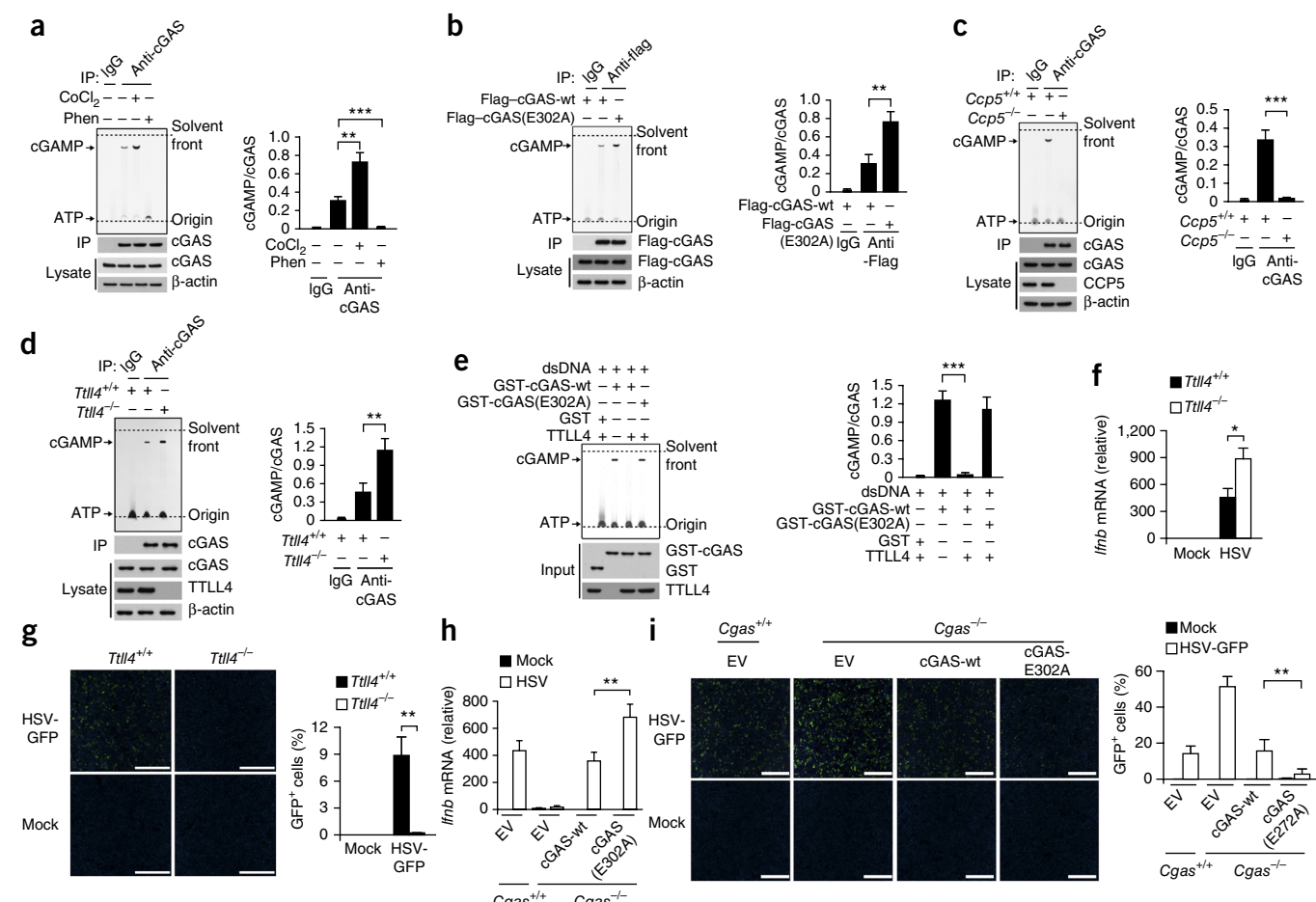


Figure 6 TTLL4-mediated monoglutamylation of cGAS blocks its synthase activity. **(a)** TLC assay of cGAS immunoprecipitated (with IgG or anti-cGAS) from wild-type BMDMs pretreated with 10 μ M CoCl₂ or 2 μ M phenanthroline (+) or not (-), in the presence of 50-base pair dsDNA, [α ³²P]ATP, GTP and MgCl₂ (top left); dashed lines indicate origin and solvent fronts (right margin). Right, ratio of cGAMP to cGAS in the samples at left. **(b)** TLC assay of BMDMs transfected for 24 h with Flag-tagged wild-type cGAS or cGAS(E302A), assessed by immunoprecipitation with anti-Flag (left), and ratio of cGAMP to cGAS in the samples at left (right). **(c,d)** TLC assay (as in a) of *Ccp5*^{+/+} and *Ccp5*^{-/-} BMDMs (c) or *Ttll4*^{+/+} and *Ttll4*^{-/-} BMDMs (d). Right, ratio of cGAMP to cGAS in the samples at left. **(e)** GST-precipitation assay and TLC assay as in a of TTLL4 incubated for 1 h with various combinations (above lanes) of dsDNA and GST or GST-tagged wild-type cGAS or cGAS(E302A) in glutamylating buffer. Right, ratio of cGAMP to cGAS in the samples at left. **(f)** RT-PCR analysis of *Ifnb* mRNA in *Ttll4*^{+/+} and *Ttll4*^{-/-} BMDMs mock infected or incubated for 8 h with HSV (MOI = 1); results are presented relative to those of mock-infected wild-type cells. **(g)** Microscopy (left) of *Ttll4*^{+/+} and *Ttll4*^{-/-} BMDMs mock infected or incubated for 24 h with HSV-GFP (MOI = 1), and frequency of GFP⁺ cells among those BMDMs (right). Scale bars (left), 400 μ m. **(h)** RT-PCR analysis of *Ifnb* mRNA in *Cgas*^{+/+} and *Cgas*^{-/-} BMDMs transfected with empty vector or vector encoding wild-type cGAS or cGAS(E302A) and mock infected or incubated for 8 h with HSV (MOI = 1); results are presented relative to those of empty vector-transfected, mock-infected wild-type cells. **(i)** Microscopy (left) of *Cgas*^{+/+} and *Cgas*^{-/-} BMDMs transfected as in h and mock infected or incubated for 24 h with HSV-GFP (MOI = 1), and frequency of GFP⁺ cells among those BMDMs (right). Scale bars (left), 400 μ m. Bottom left (a-e), immunoassay of the samples above, subjected to immunoprecipitation as above, assessed by immunoblot analysis of immunoprecipitates (IP) or total lysates (below) with anti-cGAS (a,c,d), anti-Flag (b) anti-CCP5 (c), anti-TTLL4 (d,e) and/or anti-GST (e).

*P < 0.05, **P < 0.01 and ***P < 0.001 (Student's t-test). Data are representative of at least three independent experiments (mean and s.d.).

along with vector encoding wild-type cGAS or either of the two cGAS mutants, into BMDMs for precipitation assays. More cGAS(E272A) than wild-type cGAS bound dsDNA, whereas cGAS(E302A) and wild-type cGAS bound dsDNA to a similar degree (Fig. 5c). These data suggested that glutamylation of Glu272 hindered the binding of DNA to cGAS. Additionally, cGAS did not bind dsDNA in *Ccp6*^{-/-} BMDMs (Fig. 5d,e). However, similar amounts of cGAS bound dsDNA in *Ccp5*^{-/-} and wild-type BMDMs (Fig. 5d and Supplementary Fig. 5a). Accordingly, cGAS(E302A) overexpressed in *CCP6*^{-/-} BMDMs failed to bind dsDNA (Fig. 5f), whereas cGAS(E272A) overexpressed in

CCP5^{-/-} BMDMs bound the same amount of dsDNA as in *CCP5*^{+/+} cells (Supplementary Fig. 5b). The polyglutamylation of cGAS at Glu272, therefore, suppressed its DNA-binding ability.

Given that TTLL6 catalyzed the polyglutamylation of cGAS at Glu272, we used *Ttll6*^{-/-} cells to further investigate the dsDNA-binding ability mediated by the polyglutamylation of cGAS. We noted that more cGAS was able to bind dsDNA in *Ttll6*^{-/-} BMDMs than in wild-type cells, whereas similar amounts of cGAS were precipitated by dsDNA in *Ttll4*^{-/-} BMDMs and wild-type cells (Fig. 5g). Consistent with that, overexpression of cGAS(E302A) in *Ttll6*^{-/-} BMDMs enhanced

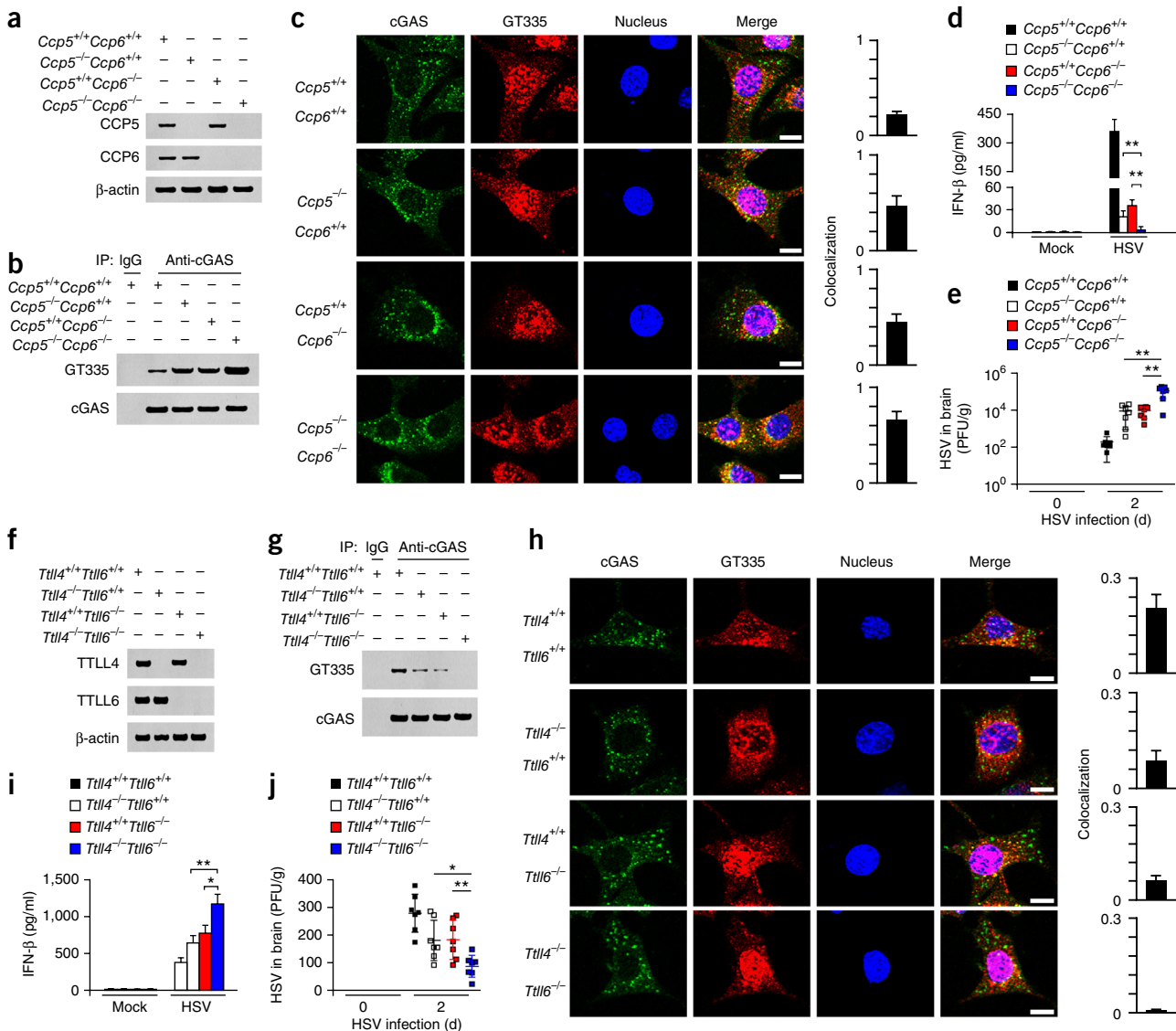


Figure 7 Glutamylation and deglutamylation of cGAS tightly modulates antiviral immunity. (a) Immunoblot analysis of CCP5 and CCP6 in BMDMs from mice deficient in *Ccp5* and/or *Ccp6* (above lanes; $n = 7$ mice per strain in a–e). (b) Immunoprecipitation of cGAS from BMDMs from mice deficient in *Ccp5* and/or *Ccp6* (above lanes), assessed by immunoblot analysis with GT335 or anti-cGAS. (c) Microscopy of BMDMs deficient in *Ccp5* and/or *Ccp6* (left margin) stained with anti-cGAS and GT335 (left), and colocalization of cGAS and GT335 signals in those cells (right). Scale bars (left), 10 μ m. (d) ELISA of IFN- β in serum from mice deficient in *Ccp5* and/or *Ccp6* (key), at 8 h after intravenous injection of vehicle (Mock) or HSV (1×10^7 PFU per mouse). (e) Viral titers in homogenates of brains from mice deficient in *Ccp5* and/or *Ccp6* (key), analyzed immediately (0 d) or 2 d after intravenous injection of HSV (1×10^6 PFU per mouse). (f) Immunoblot analysis of TTLL4 and TTLL6 in BMDMs from mice deficient in *Ttll4* and/or *Ttll6* (above lanes; $n = 7$ mice per strain in f–j). (g) Immunoprecipitation of cGAS from BMDMs deficient in *Ttll4* and/or *Ttll6* (above lanes), assessed by immunoblot analysis with GT335 or anti-cGAS. (h) Microscopy of BMDMs from mice deficient in *Ttll4* and/or *Ttll6*, stained with anti-cGAS and GT335 in those cells (left), and colocalization of cGAS and GT335 signals (right). Scale bars (left), 10 μ m. (i) ELISA of IFN- β in serum from mice deficient in *Ttll4* and/or *Ttll6* (key) at 8 h after infection as in d. (j) Viral titers in homogenates of brains deficient in *Ttll4* and/or *Ttll6*, analyzed immediately (at 0 d) or 2 d after infection as in d. * $P < 0.05$ and ** $P < 0.01$ (Student's *t*-test). Data are representative of at least three independent experiments (mean and s.d. in c–e, h–j).

its DNA-binding ability, as did overexpression of cGAS(E272A), whereas overexpression of cGAS(E302A) in *Ttll6*^{+/+} BMDMs did not affect its DNA-binding affinity (Fig. 5h). However, *Ttll4* deficiency did not affect the DNA-binding ability of cGAS (Supplementary Fig. 5c). Finally, cGAS(E272A) pre-incubated with TTLL6 *in vitro* was precipitated by dsDNA as efficiently as recombinant wild-type cGAS was, but wild-type cGAS and cGAS(E302A) lost their DNA-binding ability after incubation with TTLL6 *in vitro* (Fig. 5i,j). In contrast, incubation with TTLL4 did not alter the DNA-binding ability of cGAS(E272A) or cGAS(E302A) (Supplementary Fig. 5d). These results indicated that the TTLL6-mediated polyglutamylation of cGAS at Glu272 abolished its DNA-binding ability.

As a consequence of the results reported above, *Ttll6*^{-/-} BMDMs exhibited higher expression of *Ifnb* mRNA than that of *Ttll6*^{+/+} cells after infection with HSV (Fig. 5k). Moreover, *Ttll6* deficiency substantially suppressed the propagation of HSV (Supplementary Fig. 5e). We then generated BMDMs deficient in the gene encoding cGAS (*Mb21d1*; called 'Cgas' here) via a CRISPR-Cas9 approach, as reported⁷, and restored cGAS expression via wild-type cGAS or cGAS(E272A) in these *Cgas*^{-/-} cells. We found that restoration with cGAS(E272A) accelerated interferon expression relative to its expression after restoration with wild-type cGAS and consequently suppressed viral amplification (Supplementary Fig. 5f,g). Therefore, TTLL6-mediated polyglutamylation of cGAS at Glu272 inhibited its DNA-binding ability, which led to suppression of its activity against viral infection.

Blockade of cGAS synthase activity via monoglutamylation

We further explored how the synthase activity of cGAS was regulated by its glutamylation. We observed, by thin-layer chromatography (TLC), that treatment with CoCl₂ substantially enhanced the formation of cGAMP catalyzed by cGAS (Fig. 6a). Conversely, treatment with phenanthroline abrogated the synthesis of cGAMP (Fig. 6a), which suggested that glutamylation of cGAS participated in the negative regulation of its enzymatic activity. cGAS(E302A) promoted much more formation of cGAMP than did wild-type cGAS (Fig. 6b), which suggested that monoglutamylation of cGAS at Glu302 inhibited its synthase activity.

We observed that CCP5 removed the monoglutamylation of cGAS at Glu302 (Supplementary Fig. 4c). As expected, *Ccp5* deficiency disrupted the synthase activity of cGAS (Fig. 6c). We also found that the monoglutamylation of cGAS at Glu302 was catalyzed by TTLL4 (Fig. 4f). Therefore, *Ttll4* deficiency resulted in significantly augmented cGAMP synthesis (Fig. 6d). In addition, cGAS(E302A) still displayed cGAMP-synthetic activity after incubation with TTLL4 *in vitro*, whereas wild-type cGAS lost its cGAMP-synthetic ability after incubation with TTLL4 (Fig. 6e). These data indicated that monoglutamylation of cGAS at Glu302 catalyzed by TTLL4 impeded the synthase activity of cGAS for cGAMP synthesis.

As expected, *Ttll4*^{-/-} BMDMs displayed higher expression of *Ifnb* mRNA than that of *Ttll4*^{+/+} cells after infection with HSV (Fig. 6f). Consequently, *Ttll4* deficiency substantially suppressed the propagation of HSV (Fig. 6g). We then restored cGAS expression via wild-type cGAS or cGAS(E302A) in *Cgas*-deficient BMDMs. We found that restoration with cGAS(E302A) promoted *Ifnb* expression and consequently restricted viral propagation (Fig. 6h,i). Thus, TTLL4-mediated monoglutamylation of cGAS at Glu302 blocked its synthase activity, which resulted in suppression of its antiviral activity.

Modulation of antiviral immunity via cGAS glutamylation states

To further confirm the proposal of a role for glutamylation and deglutamylation in innate immune responses to DNA viruses,

we generated *Ccp5*^{-/-}*Ccp6*^{-/-} double-deficient mice by crossing *Ccp5*^{-/-} mice with *Ccp6*^{-/-} mice and found that the *Ccp5*^{-/-}*Ccp6*^{-/-} mice lacked expression of CCP5 and CCP6 (Fig. 7a). As expected, *Ccp5*^{-/-}*Ccp6*^{-/-} BMDMs showed augmented glutamylation of cGAS relative to that of *Ccp5*^{-/-} or *Ccp6*^{-/-} cells (Fig. 7b,c). Consequently, *Ccp5*^{-/-}*Ccp6*^{-/-} mice had a blockade in the production of IFN- β (Fig. 7d) and were highly susceptible to infection with HSV (Fig. 7e), whereas *Ccp5*^{-/-} or *Ccp6*^{-/-} mice produced some IFN- β (Fig. 7d) but had compromised resistance to infection with HSV (Fig. 7e). These data indicated that CCP5- and CCP6-mediated deglutamylation of cGAS enhanced the production of type I interferons and eradication of DNA viruses.

We also established *Ttll4*^{-/-}*Ttll6*^{-/-} double-deficient mice by crossing *Ttll4*^{-/-} mice with *Ttll6*^{-/-} mice and found that *Ttll4*^{-/-}*Ttll6*^{-/-} mice lacked expression of TTLL4 and TTLL6 (Fig. 7f). We observed that *Ttll4*^{-/-}*Ttll6*^{-/-} BMDMs lacked glutamylation of cGAS, whereas *Ttll4*^{-/-} or *Ttll6*^{-/-} cells exhibited some glutamylation of cGAS (Fig. 7g,h). Moreover, *Ttll4*^{-/-}*Ttll6*^{-/-} mice produced greater amounts of IFN- β than did *Ttll4*^{-/-} or *Ttll6*^{-/-} mice (Fig. 7i) and were much more resistant to infection with HSV than were *Ttll4*^{-/-} or *Ttll6*^{-/-} mice (Fig. 7j). Thus, TTLL4- and TTLL6-mediated glutamylation of cGAS suppressed the production of type I interferons and clearance of DNA viruses. Glutamylation and deglutamylation of cGAS, therefore, tightly regulated the immune response during infection with DNA viruses.

DISCUSSION

cGAS is a member of the nucleotidyltransferase family that catalyzes the synthesis of cGAMP from GTP and ATP in the presence of dsDNA^{15,30}. In the resting state, the catalytic regions of cGAS are embedded inside cGAS, which hinders the catalytic generation of cGAMP from ATP and GTP^{16,31,32}. Once bound to DNA, cGAS undergoes a conformational change that renders the catalytic pocket of cGAS accessible for cGAMP synthesis^{28,29,33}. Collectively, such studies suggest that engagement of DNA is a prerequisite for activation of the nucleotidyltransferase activity of cGAS. Here we found that the activity of cGAS was tightly regulated by glutamylation and deglutamylation, which had a critical role in the modulation of innate immune responses.

Post-translational modifications act as regulatory signals for control of the stability, localization, activity and function of proteins^{20,25,34,35}. Glutamylation is a modification that adds monoglutamic or polyglutamic acid residues to target proteins in an ATP-dependent manner^{20,21,35}. Glutamylation is catalyzed by the TTLL family of glutamylases²². Glutamylation was originally identified on tubulins as a dominant tubulin modification in the adult brain of mammals³⁶. Tubulins and nucleosome-assembly proteins are well-known substrates for polyglutamylation^{21,35}. In this study, we found that TTLL4 and TTLL6 glutamylated the previously unknown substrate cGAS differentially. TTLL6-mediated polyglutamylation of cGAS at Glu272 impeded its DNA-binding ability, whereas TTLL4-mediated monoglutamylation of cGAS at Glu302 blocked its synthase activity. Of note, TTLL glutamylases differ in their 'preferences' for their substrates, as well as for the catalysis of glutamate chains, side-chain initiation or elongation²³. Thus, TTLL glutamylases direct their effects to different target substrates.

Glutamylation is a reversible modification, and deglutamylation is hydrolyzed by CCPs^{21,34,37}. Members of the CCP family have specific expression profiles in different tissues and are involved in a variety of physiological functions^{21,38}. Members of this family have 'preferred' enzymatic specificities for hydrolyzing deglutamylation. Among these

members, CCP1, CCP4 and CCP6 remove the shortening of penultimate polyglutamate chains of α -tubulin, while CCP5 specifically hydrolyzes the branching site glutamate²¹. Our results indicated non-redundant roles for CCP5 and CCP6 in the regulation of cGAS activity. Of note, we observed that the amount of glutamylated cGAS diminished rapidly after infection with HSV. Meanwhile, the amount of TTLL4 and TTLL6 protein decreased substantially after infection with HSV, whereas the amount of CCP5 and CCP6 remained unchanged during the process of infection. Moreover, after infection with HSV, cGAS associated with larger amounts of CCPs but smaller amounts of TTLL glutamylases. These observations suggested that the activity of cGAS was tightly regulated by its dynamic glutylation and deglutylation modifications during infection with HSV.

cGAS detects cytosolic DNA in a sequence-independent manner, which elicits the cGAS-STING pathway to prime innate immune responses to various DNA viruses, retroviruses and even bacterial pathogens^{39–41}. Manipulating the glutylation state of cGAS could thus potentially either initiate the cGAS-STING pathway to eradicate DNA viruses or shut down this pathway to prevent excessive immune responses. Together our findings have shown that the glutylation and deglutylation of cGAS regulated its activity and, as a consequence, controlled the response to DNA viruses. Therefore, manipulation of the glutylation state of cGAS might be of clinical importance.

METHODS

Methods and any associated references are available in the [online version of the paper](#).

Note: Any Supplementary Information and Source Data files are available in the online version of the paper.

ACKNOWLEDGMENTS

We thank S. Meng, J. Cheng, M. Ding, J. Wang, X. Gao, X. Zhang, L. Zhou, X. Wu, J. Hao, D. Liu, J. Jia, C. Jiang and . Teng for technical support; J. Bennink (National Institute of Allergy and Infectious Diseases) for vesicular stomatitis virus and VACV strains; H. Peng (Institute of Biophysics, Chinese Academy of Sciences) for Vero cells and HSV-1f virus. Supported by the National Natural Science Foundation of China (31530093, 91419308, 31300645, 31471386 and 31570892), the Strategic Priority Research Programs of the Chinese Academy of Sciences (XDA01010407 and XDA01020203), the Youth Innovation Promotion Association of Chinese Academy of Sciences (S.W.) and the China Postdoctoral Science Foundation (2015M571141 to P.X.).

AUTHOR CONTRIBUTIONS

P.X. designed and performed experiments, analyzed data and wrote the paper; B.Y. and S.W. performed experiments and analyzed data; X.Z. generated mutant mice; Y.D. and Z.X. performed some experiments; Y.T. initiated the study and analyzed data; and Z.F. initiated the study, and organized, designed and wrote the paper.

COMPETING FINANCIAL INTERESTS

The authors declare no competing financial interests.

Reprints and permissions information is available online at <http://www.nature.com/reprints/index.html>.

- Wu, J. & Chen, Z.J. Innate immune sensing and signaling of cytosolic nucleic acids. *Annu. Rev. Immunol.* **32**, 461–488 (2014).
- Kumar, H., Kawai, T. & Akira, S. Pathogen recognition by the innate immune system. *Int. Rev. Immunol.* **30**, 16–34 (2011).
- Xia, P. *et al.* IRKTS negatively regulates antiviral immunity through PCBP2 sumoylation-mediated MAVS degradation. *Nat. Commun.* **6**, 8132 (2015).
- Hou, F. *et al.* MAVS forms functional prion-like aggregates to activate and propagate antiviral innate immune response. *Cell* **146**, 448–461 (2011).
- Loo, Y.M. & Gale, M. Jr. Immune signaling by RIG-I-like receptors. *Immunity* **34**, 680–692 (2011).
- Meylan, E. *et al.* Cardif is an adaptor protein in the RIG-I antiviral pathway and is targeted by hepatitis C virus. *Nature* **437**, 1167–1172 (2005).
- Xia, P. *et al.* Sox2 functions as a sequence-specific DNA sensor in neutrophils to initiate innate immunity against microbial infection. *Nat. Immunol.* **16**, 366–375 (2015).
- Bauer, M. *et al.* Bacterial CpG-DNA triggers activation and maturation of human CD11c⁺ CD123⁺ dendritic cells. *J. Immunol.* **166**, 5000–5007 (2001).
- Hornung, V. *et al.* AIM2 recognizes cytosolic dsDNA and forms a caspase-1-activating inflammasome with ASC. *Nature* **458**, 514–518 (2009).
- Takaoka, A. *et al.* DAI (DLM-1/ZBP1) is a cytosolic DNA sensor and an activator of innate immune response. *Nature* **448**, 501–505 (2007).
- Unterholzner, L. *et al.* IFI16 is an innate immune sensor for intracellular DNA. *Nat. Immunol.* **11**, 997–1004 (2010).
- Zhang, Z. *et al.* The helicase DDX41 senses intracellular DNA mediated by the adaptor STING in dendritic cells. *Nat. Immunol.* **12**, 959–965 (2011).
- Ablasser, A. *et al.* Cell intrinsic immunity spreads to bystander cells via the intercellular transfer of cGAMP. *Nature* **503**, 530–534 (2013).
- Li, X.D. *et al.* Pivotal roles of cGAS-cGAMP signaling in antiviral defense and immune adjuvant effects. *Science* **341**, 1390–1394 (2013).
- Sun, L., Wu, J., Du, F., Chen, X. & Chen, Z.J. Cyclic GMP-AMP synthase is a cytosolic DNA sensor that activates the type I interferon pathway. *Science* **339**, 786–791 (2013).
- Ablasser, A. *et al.* cGAS produces a 2-5-linked cyclic dinucleotide second messenger that activates STING. *Nature* **498**, 380–384 (2013).
- Hornung, V., Hartmann, R., Ablasser, A. & Hopfner, K.P. OAS proteins and cGAS: unifying concepts in sensing and responding to cytosolic nucleic acids. *Nat. Rev. Immunol.* **14**, 521–528 (2014).
- Gay, N.J., Symmons, M.F., Gangloff, M. & Bryant, C.E. Assembly and localization of Toll-like receptor signalling complexes. *Nat. Rev. Immunol.* **14**, 546–558 (2014).
- Popovic, D., Vucic, D. & Dikic, I. Ubiquitination in disease pathogenesis and treatment. *Nat. Med.* **20**, 1242–1253 (2014).
- Garnham, C.P. *et al.* Multivalent microtubule recognition by tubulin tyrosine ligase-like family glutamylases. *Cell* **161**, 1112–1123 (2015).
- Rogowski, K. *et al.* A family of protein-deglutamylating enzymes associated with neurodegeneration. *Cell* **143**, 564–578 (2010).
- Janke, C. *et al.* Tubulin polyglutamylase enzymes are members of the TTL domain protein family. *Science* **308**, 1758–1762 (2005).
- van Dijk, J. *et al.* A targeted multienzyme mechanism for selective microtubule polyglutamylation. *Mol. Cell* **26**, 437–448 (2007).
- Kubo, T., Yanagisawa, H.A., Yagi, T., Hiroto, M. & Kamiya, R. Tubulin polyglutamylation regulates axonemal motility by modulating activities of inner-arm dyneins. *Curr. Biol.* **20**, 441–445 (2010).
- Ye, B. *et al.* Cytosolic carboxypeptidase CCP6 is required for megakaryopoiesis by modulating Mad2 polyglutamylation. *J. Exp. Med.* **211**, 2439–2454 (2014).
- Chiu, Y.H., Macmillan, J.B. & Chen, Z.J. RNA polymerase III detects cytosolic DNA and induces type I interferons through the RIG-I pathway. *Cell* **138**, 576–591 (2009).
- Bereznik, I. *et al.* Cytosolic carboxypeptidase 1 is involved in processing α - and β -tubulin. *J. Biol. Chem.* **287**, 6503–6517 (2012).
- Civril, F. *et al.* Structural mechanism of cytosolic DNA sensing by cGAS. *Nature* **498**, 332–337 (2013).
- Gao, P. *et al.* Cyclic [G(2,5)pA(3,5)p] is the metazoan second messenger produced by DNA-activated cyclic GMP-AMP synthase. *Cell* **153**, 1094–1107 (2013).
- Gao, D. *et al.* Cyclic GMP-AMP synthase is an innate immune sensor of HIV and other retroviruses. *Science* **341**, 903–906 (2013).
- Ahn, J. & Barber, G.N. Self-DNA, STING-dependent signaling and the origins of autoinflammatory disease. *Curr. Opin. Immunol.* **31**, 121–126 (2014).
- Schoggins, J.W. *et al.* Pan-viral specificity of IFN-induced genes reveals new roles for cGAS in innate immunity. *Nature* **505**, 691–695 (2014).
- Kranzusch, P.J., Lee, A.S., Berger, J.M. & Doudna, J.A. Structure of human cGAS reveals a conserved family of second-messenger enzymes in innate immunity. *Cell Rep.* **3**, 1362–1368 (2013).
- Bereznik, I. *et al.* CCP1/Nna1 functions in protein turnover in mouse brain: Implications for cell death in Purkinje cell degeneration mice. *FASEB J.* **24**, 1813–1823 (2010).
- Garnham, C.P. & Roll-Mecak, A. The chemical complexity of cellular microtubules: tubulin post-translational modification enzymes and their roles in tuning microtubule functions. *Cytoskeleton* **69**, 442–463 (2012).
- Janke, C., Rogowski, K. & van Dijk, J. Polyglutamylation: a fine-regulator of protein function? Protein Modifications: beyond the usual suspects' review series. *EMBO Rep.* **9**, 636–641 (2008).
- Rodríguez de la Vega Otazo, M., Lorenzo, J., Tort, O., Aviles, F.X. & Bautista, J.M. Functional segregation and emerging role of cilia-related cytosolic carboxypeptidases (CCPs). *FASEB J.* **27**, 424–431 (2013).
- Fernandez-Gonzalez, A. *et al.* Purkinje cell degeneration (pcd) phenotypes caused by mutations in the axotomy-induced gene, Nna1. *Science* **295**, 1904–1906 (2002).
- Collins, A.C. *et al.* Cyclic GMP-AMP Synthase is an innate immune DNA sensor for *Mycobacterium tuberculosis*. *Cell Host Microbe* **17**, 820–828 (2015).
- Wassermann, R. *et al.* *Mycobacterium tuberculosis* differentially activates cGAS- and inflammasome-dependent intracellular immune responses through ESX-1. *Cell Host Microbe* **17**, 799–810 (2015).
- Watson, R.O. *et al.* The cytosolic sensor cGAS detects *Mycobacterium tuberculosis* DNA to induce type I interferons and activate autophagy. *Cell Host Microbe* **17**, 811–819 (2015).

ONLINE METHODS

Antibodies and reagents. Antibodies used were as follows: anti-CCP1 (LM-1A7), anti-CCP2 (S-13), anti-CCP3 (S-15), anti-CCP4 (T-17), anti-CCP5 (N-18), anti-CCP6 (N-14), anti-TTLL4 (S-14), anti-cGAS (N-17), anti-IRF3 (D-3), anti- β -tubulin, anti-TBK1 (M-375), anti-STING (M-12) and anti-Myc (9E10) (all from Santa Cruz Biotechnology); polyclonal anti-TTLL4 (PAB22002) and polyclonal anti-TTLL6 (H00284076-K) (both from Abnova); antibody to the polyglutamylated modification (GT335) and antibody to the polyglutamate chain (polyE) (IN105) (both from Adipogen); and polyclonal anti-GST (G7781), anti-Flag (M1), anti-His (6AT18) and anti- β -actin (SP124) (all from Sigma-Aldrich). The secondary antibody donkey anti-rabbit IgG conjugated to Alexa Fluor 488 (A11008), Alexa Fluor 594 (A11012) or Alexa Fluor 405 (A31556) and secondary antibody donkey anti-mouse IgG conjugated to Alexa Fluor 488 (A11029) or Alexa Fluor 594 (A11032) were purchased from Molecular Probes. Paraformaldehyde (PFA), phenanthroline, CoCl₂ and DAPI (4,6-diamidino-2-phenylindole) were from Sigma-Aldrich.

Cells and culture. BMDMs were generated as described below. Bone marrow cells aspirated from mouse femurs were cultured for 7 d in RPMI-1640 medium containing 10% FBS and 50 ng/ml macrophage colony-stimulating factor. For macrophage transfection, BMDMs (1×10^6) were resuspended in 100 μ l Nucleofector Solution buffer (Lonza) containing 5 μ g DNA or other substrates, followed by transfection using the Nucleofector Program Y-001 on Amaxa nucleofector II device (Lonza). Cells were recovered for 6 h in RPMI-1640 medium containing 4 mM L-glutamine, 1.5 g/l sodium bicarbonate and 10% heat-inactivated FBS, followed sorting of viable cells by flow cytometry. To exclude the possible effects of transfected DNAs on subsequent experiments, plasmids transfected cells were further cultured for 48 h to allow stable exogenous gene expression for further examination as described³⁰. Cells tested negative for mycoplasma contamination.

Animals and viruses. Mouse experiments complied with ethical regulations and were approved by the Institutional Animal Care and Use Committees at the Institute of Biophysics, Chinese Academy of Sciences. *Ccp1*- or *Ccp6*-deficient mice were described previously²⁵. *Ccp2*-, *Ccp3*-, *Ccp4*-, *Ccp5*-, *Tll4*- or *Tll6*-deficient mouse strains were generated using CRISPR-Cas9 approaches as described⁴². Vesicular stomatitis virus and VACV virus strains were gifts from J. Bennink (National Institute of Allergy and Infectious Diseases). The viral strain HSV-1f was a gift from H. Peng (Institute of Biophysics, Chinese Academy of Sciences). For preparation of virus, viruses were incubated with Vero cells, followed by supernatant collection 48 h later. Supernatants were ultra-centrifuged at 25,000g for 2 h. Pellets were resuspended in RPMI-1640 medium. For virus infection *in vivo*, mice were given intravenous injection of virus or were inoculated intranasally with virus. Viruses were injected intravenously into mice for determination of viral load in brain.

Plasmid construction and protein purification. cDNA was cloned from a bone marrow cDNA library⁷. cDNA encoding CCP5, CCP6, TTLL4 or TTLL6 was subcloned to pFlag-CMV2 (Sigma-Aldrich) or pcDNA4/TO/myc-His B (Invitrogen) for expression in mammalian cells. Protein mutants were generated by site-directed mutagenesis method as previously described²⁵. cDNAs encoding CCPs and TTLL glutamylases were subcloned into a modified pGEX-6P-1 vector (GE Healthcare) with a carboxy-terminal six-histidine tag. Plasmids were transformed into *Escherichia coli* strain BL21 (DE3). DE3 clones were cultured (absorbance at 600 nm, 0.6), followed by induction with 0.2 mM IPTG at 16 °C for 24 h. Cells were collected and lysed through the use of an ultrasonic cell disruptor followed by successive purification through Ni-NTA resins and GST resins.

Immunoprecipitation assay. Cells were lysed in lysis buffer containing 150 mM NaCl, 50 mM Tris-Cl, 1% TritonX-100 and protease inhibitor cocktail, pH 7.4. Lysates were centrifuged on 15,000g for 15 min at 4 °C, and supernatants were incubated for 6 h at 4 °C with the appropriate antibodies (identified above), followed by immunoprecipitation with 20 μ l protein A/G-conjugated agarose (Santa Cruz Biotechnology). Precipitates were completely washed with lysis buffer and separated by SDS-PAGE, followed by transfer to nitrocellulose membranes and immunoblot analysis.

Immunofluorescence Immunostaining was performed as described previously⁴³. Cells were plated on 0.01% poly-L-lysine treated coverslips and fixed with 4% PFA for 10 min, followed by permeabilization with 0.5% Triton X-100 for 20 min at room temperature. Primary antibodies (identified above) were added for 2 h, followed by further staining with Alexa Fluor 488- or Alexa Fluor 594-conjugated secondary antibodies (identified above). Cells were visualized by confocal microscopy (Olympus FV1000).

AlphaScreen. Purified cGAS variants and biotinylated DNA were incubated at various concentrations according to the manufacturer's instructions (AlphaScreen; PerkinElmer)⁷.

DNA-precipitation assay **DNA-precipitation assays were performed as previously described⁴⁴.** dsDNA was synthesized with an NH₂ modification at the 5' end and the two complementary sequences were annealed, followed by coupling to CNBr-activated Sepharose 4B resins (GE Healthcare). For the DNA-precipitation assay, recombinant proteins or cell lysates were incubated with DNA-linked resins in the presence of Protease Inhibitor Cocktail Set III (Calbiochem), followed by washing with buffer containing 150 mM KCl, and immunoblot analysis (as described above) of precipitates.

Chromatin immunoprecipitation. BMDMs overexpressing Flag-tagged cGAS variants were transfected with dsDNA, followed by crosslinking with 1% formaldehyde at 37 °C for 10 min. Lysates were incubated with anti-Flag for 6 h after preclearance with salmon sperm DNA-protein A agarose. Flag-tagged cGAS was then immunoprecipitated by salmon sperm DNA-protein A agarose. Immunoprecipitates were washed sequentially with low-salt wash buffer, high-salt wash buffer, LiCl wash buffer, and TE buffer, followed by eluting with elution buffer (1% SDS and 0.1 M NaHCO₃). The cGAS-DNA complex was reversed by heating at 65 °C for 4 h. DNA was further purified by phenol-chloroform extraction and precipitated with ethanol, followed by RT-PCR analysis.

RT-PCR analysis. Total RNA was extracted from cells using Trizol reagent and cDNA was reverse-transcribed using Superscript II (Invitrogen). RT-PCR was performed using a StarScript II Two-step RT-PCR Kit (Genestar) with the following primers: *Ifna* primers, sense, 5'-ACTCATAACCTCAGGAACAAG-3', and anti-sense, 5'-CTTGATGTGAAGATGTTAG-3'; *Ifnb* primers, sense, 5'-AGTACAACAGCTACGCCCTGG-3', and anti-sense, 5'-GAGTCC GCCTCTGATGCTTA-3'; *Ccp1*: sense, 5'-GGGGTCGAAGAGCAGTT-3', and anti-sense, 5'-GAATGGAGTGGAGTCTGCACCA-3'; *Ccp2*: sense, 5'-ATGA ATGTCCTGCTTGAGATG-3', and anti-sense, 5'-CAAACCGCCTGATGA GTGC-3'; *Ccp3*: sense, 5'-AGCTGAAGATG CTTACAAAGAGC-3', and anti-sense, 5'-CGCACAGTCAACTCGTATTAT-3'; *Ccp4*: sense, 5'-CCAGCA GTGCCTATACTCTCC-3', anti-sense, 5'-TGCTCAGATCAGTTCCAAGT C-3'; *Ccp5*: sense, 5'-CTGCTCATTCTCGTCTTCAGG-3', and anti-sense, 5'-ATCGAGTCCT AATGCAAGGGA-3'; and *Ccp6*: sense, 5'-AGGCAGGCA ATGATACAGGAA-3', and anti-sense, 5'-GGTTACCACCTTCAAAGCAAGCA-3'.

In vitro glutamylayation assay. Flag-tagged TTLL4 or TTLL6 was overexpressed in mouse embryonic fibroblasts, followed by immunoprecipitation with anti-Flag. Immunoprecipitates were eluted with Flag peptides, followed by incubation with recombinant cGAS in glutamylayation buffer containing 50 mM Tris-HCl, 5 mM MgCl₂, 2.5 mM dithiothreitol, 10 mM sodium glutamate and 2 mM ATP, pH 7.0. Reactions were incubated at 30 °C for 1 h.

Statistical analysis. Student's *t*-test was used for statistical analysis by using Microsoft Excel⁴⁵.

42. Zhu, X. *et al.* An efficient genotyping method for genome-modified animals and human cells generated with CRISPR/Cas9 system. *Sci. Rep.* **4**, 6420 (2014).
43. Xia, P. *et al.* WASH inhibits autophagy through suppression of Beclin 1 ubiquitination. *EMBO J.* **32**, 2685–2696 (2013).
44. Wang, S. *et al.* Transient activation of autophagy via Sox2-mediated suppression of mTOR is an important early step in reprogramming to pluripotency. *Cell Stem Cell* **13**, 617–625 (2013).
45. Xia, P. *et al.* WASH is required for the differentiation commitment of hematopoietic stem cells in a c-Myc-dependent manner. *J. Exp. Med.* **211**, 2119–2134 (2014).

Erratum: Glutamylation of the DNA sensor cGAS regulates its binding and synthase activity in antiviral immunity

Pengyan Xia, Buqing Ye, Shuo Wang, Xiaoxiao Zhu, Ying Du, Zhen Xiong, Yong Tian & Zuse Fan

Nat. Immunol.; doi:10.1038/ni.3356; corrected online 29 February 2016

In the version of this article initially published online, the title of the legend to Figure 1 (“Mice deficient in CCP5 or CCP5 are susceptible to infection with DNA viruses”) was incorrect. The title should be “Mice deficient in CCP5 or CCP6 are susceptible to infection with DNA viruses.” The error has been corrected for the print, PDF and HTML versions of this article.